Supporting Information

High performance single-crystalline organic field-effect transistors based on molecular-modified dibenzo[a,e] -pentalenes derivatives

Fan Yin, [a] Long Wang, [c] Xiankai Yang, [b] Meihui Liu, [b] Hua Geng, [b] Yi Liao, [b] Qing Liao*[b] and Hongbing Fu*[ab]

[a] Tianjin Key Laboratory of Molecular Optoelectronic Sciences, School of Chemical Engineering and Technology, Tianjin University, and Collaborative Innovation Center of Chemical Science and Engineering (Tianjin), Tianjin 300072, P. R. China
[b] Department of Chemistry, Capital Normal University, Beijing, 100048, P. R., China
[c] Key Laboratory for Interface Sciences and Engineer in Advanced Materials, Ministry of Education, Taiyuan University of Technology, Taiyuan 030024, P. R. China
*E-mail: liaoqing@cnu.edu.cn; hongbing.fu@iccas.ac.cn

Keywords: dibenzo[a,e]pentalenes, single crystal, charge transport, hole mobility

Experimental details

1. Compound synthesis of TEP and OSDP

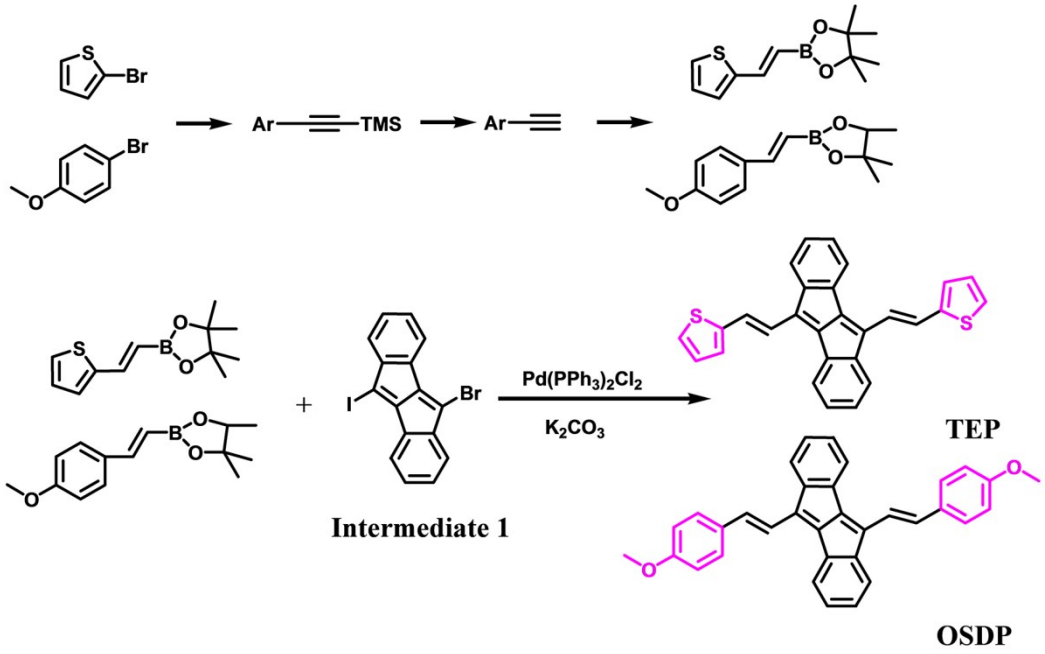

Scheme S1. Synthetic route for **TEP** and **OSDP.**

In our experiment, compounds TEP and OSDP were synthesized according to literature procedures. The synthetic intermediates **Ethylene boric acid ester** were prepared according to the literature (*J. Zhao, et al. Chem. Commun., **2014**, 50, 2058-2060*). The **intermediate 1** were prepared following the same procedures as described previously (*F. Xu, et al. Orgc. lett., **2012**, 15, 3970-3973*). Products **TEP** and **OSDP** were synthesized via Suzuki coupling reaction. The solvents were of chromatographic grade and were used as received.

5, 10-bis((E)-2-(thiophen-2-yl)vinyl)indeno[2,1-a]indene (**TEP**): Black powder solid. ^{1}H NMR (600 MHz, C_4D_8O): δ 7.62-7.63 (m, 2H), 7.56-7.57 (m, 2H), 7.53-7.56 (d, *J* = 16.6 Hz, 2H), 7.45-7.47 (m, 6H), 7.33-7.36 (d, *J* = 16.4 Hz, 2H), 6.96-7.00 (m, 4H); ^{13}C NMR (150 MHz, C_4D_8O): δ 148.03, 143.68, 140.56, 136.17, 135.74, 129.12, 126.99, 126.95, 126.26, 124.85, 124.50, 122.77, 122.43, 120.93; HR-MS (MALDI-MS): m/z=418.0845. Elem. Anal. calcd for ($C_{28}H_{18}S_2$): C, 80.38; H, 4.31; S, 15.31; found: C, 80.72; H, 4.29; S, 14.99

[4'-(methoxyl)styryl] dibenzopentalene (OSDP): Dark red powder solid. ^{1}H NMR (600 MHz, CD_2Cl_2): δ 3.86(s, 6H), 6.96-6.97(m, 4H),7.02-7.04 (m, 4H),7.27-7.30 (m, 2H) 7.42-7.43 (m, 2H), 7.57-7.58 (m, 4H); ^{13}C NMR (101 MHz, CD_2H_2): δ

160.44, 136.35, 135.80, 134.56, 129.94, 128.38, 127.28, 127.17, 122.94, 122.54, 119.13, 114.38, 55.41. HR-MS (EI) m/z: [M+] calcd. for $C_{34}H_{26}O_2$, 466.1476; found, 466.1475. Elem. Anal. calcd for ($C_{34}H_{26}O_2$): C, 87.55; H, 5.58; O, 6.87; found: C, 87.72; H, 5.49; O, 6.79

2. Fabrication of single-crystal microribbons (MRs) of TEP and OSDP

Highly n-doped (100) Si wafers (0.05–0.2U·cm) with a 300 nm-thick SiO_2 layer were successively cleaned with piranha solution (70/30 vol./vol. H_2SO_4/H_2O_2), deionized water and isopropanol, respectively, and then were dried by N_2 and O_2 plasma for 10 min. The cleaned wafers were spincoated with 1 wt% solution of polystyrene in toluene. The thickness of the polystyrene film was 30 nm. The substrate was annealing in air atmosphere at 75 ℃ for more than one night, and then the TEP and OSDP were laminated on it. The starting organic powders (typically much less than 0.5 mg) were put dispersedly. Then the substrates were placed on the hot stage, with a tiny space between the bottom and top ones separated by one small glass sleepers. The growth procedure was implemented by heating the bottom substrate to sublime the materials and formation of microcrystals on the down surface of the top substrate. The crucial parts of this method to obtain high quality single crystals are the spacing distance between the two substrates and setting suitable temperatures, which were found to be pivotal factors in determining the morphology of the grown crystals. The spacing distance of the two substrates were set at 170 μm in typical growth setup configuration of the text part (as shown in Scheme S2), where micrometer-scale single crystals of TEP and OSDP grew uniformly on the down surface of the top substrate under the condition of 220 ℃ and 200 ℃ respectively. The single-crystal microribbons (MRs) could be found on the surface of the 30 nm PS-modified SiO_2/Si wafers.

3. Structural and electronic characterization

The TEP and OSDP MR samples were characterized by field emission scanning electron microscopy (S-4800, Hitachi) by dropping on a silicon wafer. The height of microcrystals was measured by atomic force microscopy (AFM, Santa Barbara, CA). Samples examined by transmission electron microscopy (TEM, JEM-1011, JEOL) were obtained by transferring two samples on a carbon-coated copper grid. TEM measurement was performed at room temperature at an accelerating voltage of 100 kV. X-ray diffraction (XRD) patterns were measured by a D/max 2400 X-ray diffractometer with Cu Kα radiation (λ = 1.54050 Å) operated in the 2θ range from 5 to 40°, by using

the samples on a cleaned silicon substrates. Electrochemical measurements (CV) was performed with a CHI660C electrochemistry station in acetonitrile solution with sample concentration of 10^{-3} M using Bu_4NPF_6 as electrolyte, and using Pt as working electrode, platinum wire as auxiliary electrode, and a porous glass wick Ag/AgCl as pseudo-reference electrode. UPS measurements were recorded on a KRATOS Axis Ultra DLD spectrometer. The samples for UPS measurement were prepared by depositing a thin film (20 nm) of TEP and OSDP on a small plate of ITO (size: 1cm×1cm). Thermal gravimetric analysis (TGA) was performed on a STA 409 PC thermogravimeter in air at a heating rate of 10 ℃ min^{-1}. Differential scanning calorimetry was carried on a Q2000 (TA Instruments, USA) under air atmosphere.

A top-contact/bottom-gate configuration was used to fabricate TEP and OSDP crystal-based OFET devices. The source and drain electrodes (Au, 50 nm thick) were evaporated and copper grids were used as the mask. The current-voltage (I–V) curves were recorded with a Keithley 4200 SCS analyzer. All measurements were performed at room temperature in air. The mobility in the saturation region was calculated by using of the following equation: $\mu_{sat} = 2L\left(\partial\sqrt{I_{DS}}/\partial V_{GS}\right)^2/WC_i$

where Ci is the capacitance per unit area of the gate dielectric, W is the channel width and L is the channel length. The gate capacitance of the hybrid PS/SiO2 structure was calculated using $C_i=1/[1/C_1+1/C_2]$ (Wang, Y.; Kumashiro, R.; Li, Z.; Nouchi, R.; Tanigaki, K., *Applied Physics Letters* **2009**, 95,103306, Kunii, M.; Iino, H.; Hanna, J.-I., *IEEE Electron Device Letters* **2016**, *37*, 486-488.), set C_1 as the capacitance of 30nm-PS, set C_2 as the capacitance of 300nm-SiO_2. The gate capacitance of the hybrid PS/SiO2 structure was 10 nF/cm^2.

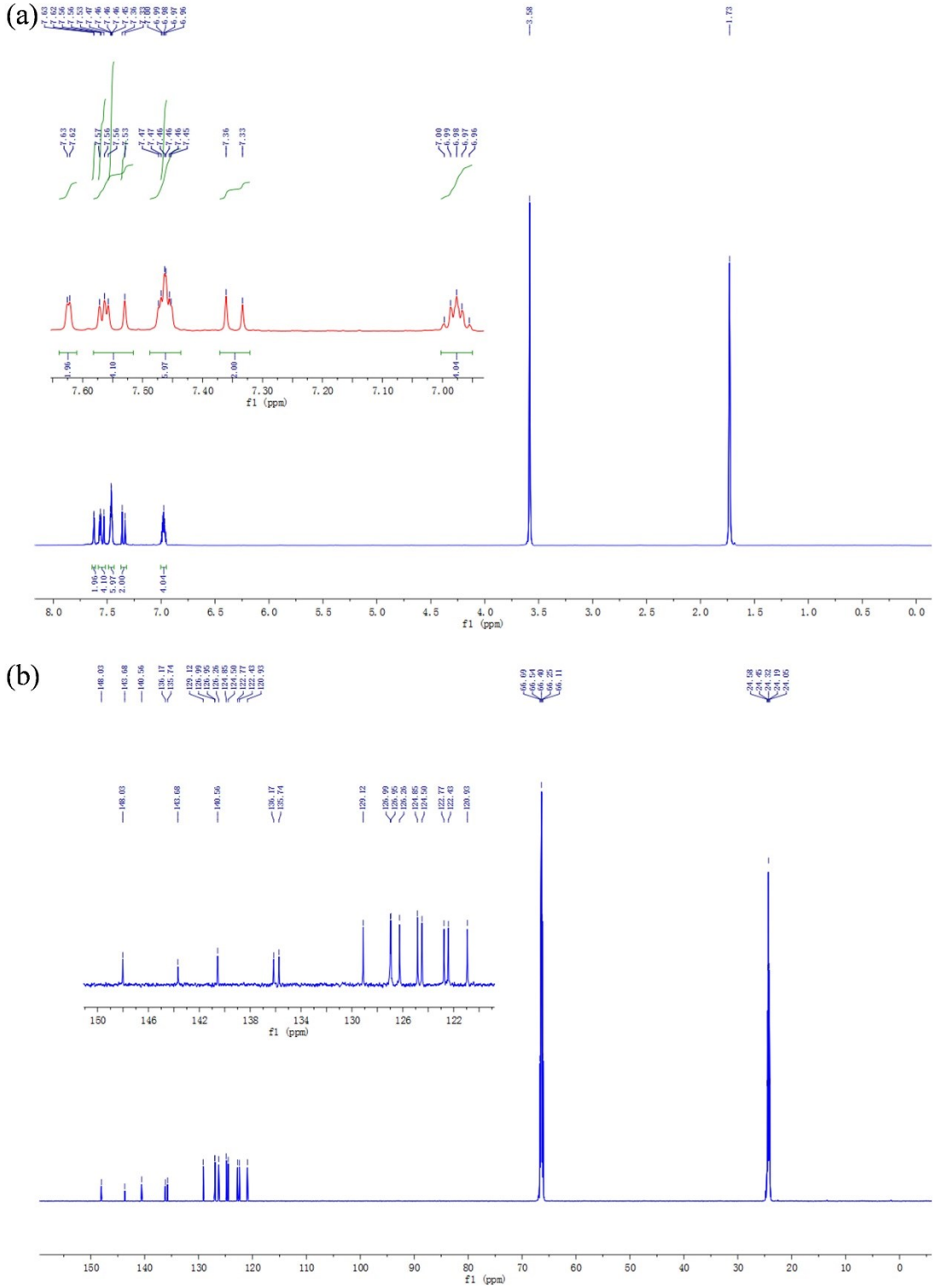

Figure S1 (a) ^{1}H-NMR spectrum of **TEP** in C_4D_8O. (b) ^{13}C-NMR spectrum of **TEP** in C_4D_8O.

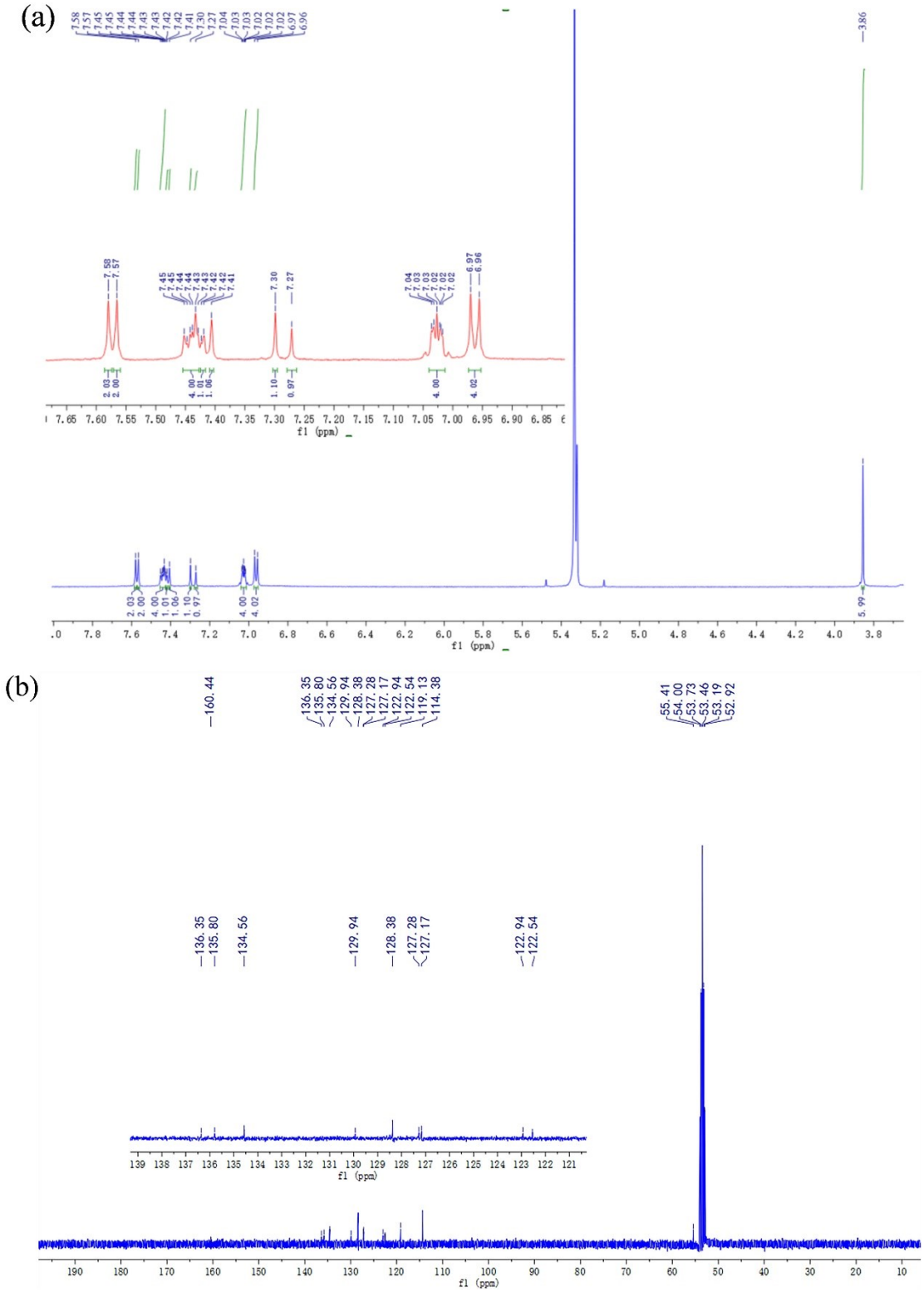

Figure S2 (a) ^{1}H-NMR spectrum of **OSDP** in CD_2Cl_2. (b) ^{13}C-NMR spectrum of **OSDP** in CD_2Cl_2.

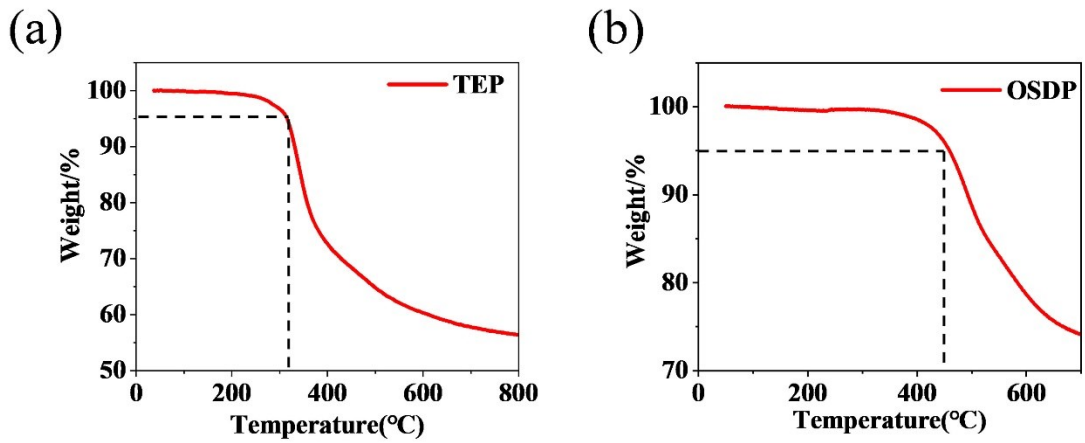

Figure S3 Thermal gravimetric analysis of TEP (a) and OSDP (b).

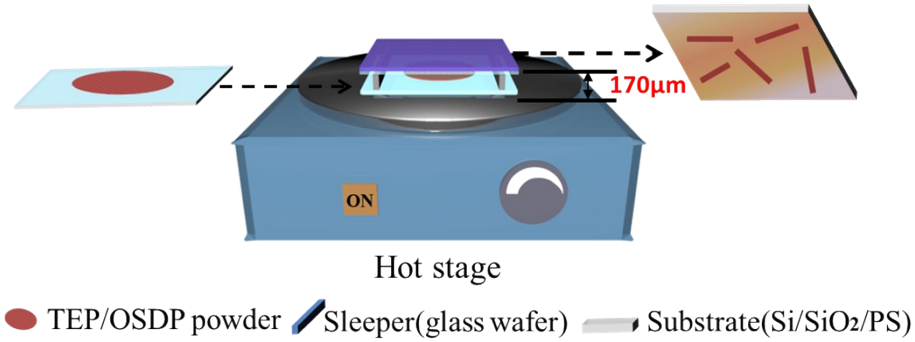

Scheme S2 Schematic drawing of the setup for crystal growth, which consists of a hot stage and two kinds of substrates separated by small glass sleepers with a spacing distance of 170 μm.

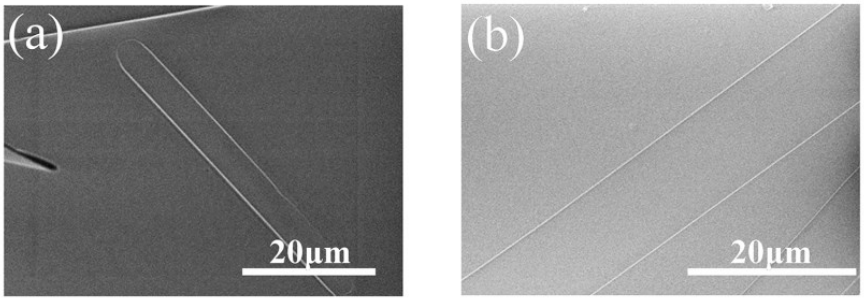

Figure S4 Scanning electron microscopy (SEM) images of TEP MRs (a) and OSDP ones (b).

Table S1 Crystal date and structure refinement for TEP and OSDP.

Name	TEP crystal (CCDCno.18280001)	OSDP crystal(CCDCno.1580864)
Empirical formula	C28 H18 S2	C34 H26 O2
Formula weight	418.54	466.55
Temperature	173.15 K	293(2) K
Wavelength	0.71073 A	0.71073 Å
Crystal system	Monoclinic	Triclinic
Space group	C 1 2/c 1	P -1
Cell Lengths (Å)	a = 22.064(9) Å b = 5.688(2) Å c = 16.512(7) Å	a = 5.2200(10) Å b = 10.511(2) Å c = 11.768(2) Å
Cell Angles (º)	a = 90° b = 105.246(4)° c = 90°	a =70.25° b= 80.71(3)° c = 80.17(3)°
Volume	1999.3(13) Å^3	595.0(2) Å^3
Z	4	1
Density (calculated)	1.391 Mg/m^3	1.302 Mg/m^3
Absorption coefficient	0.280 mm^-1	0.079 mm^-1
F(000)	872	246
Theta range for data collection	2.557 to 27.507 °	1.850 to 27.487°
Limiting indices	-28<=h<=28, -7<=k<=7, -21<=l<=21	-6<=h<=6, -13<=k<=13, -15<=l<=15
Reflections collected	7817	8276
Independent reflections	2282 [R(int) = 0.0407]	2719 [R(int) = 0.0470]
Refinement method	Full-matrix least-squares on F^2	Full-matrix least-squares on F^2
Data / restraints / parameters	2282 / 263 / 200	2719 / 0 / 164
Goodness-of-fit on F2	1.177	1.194
Final R indices [I>2sigma(I)]	R1 = 0.0587, wR2 = 0.1305	R1 = 0.0648, wR2 = 0.1389
R indices (all data)	R1 = 0.0631, wR2 = 0.1330	R1 = 0.0726, wR2 = 0.1433
Extinction coefficient	n/a	n/a
Largest diff. peak and hole	0.271 and -0.257 e.Å^-3	0.220 and -0.210 e.Å^-3

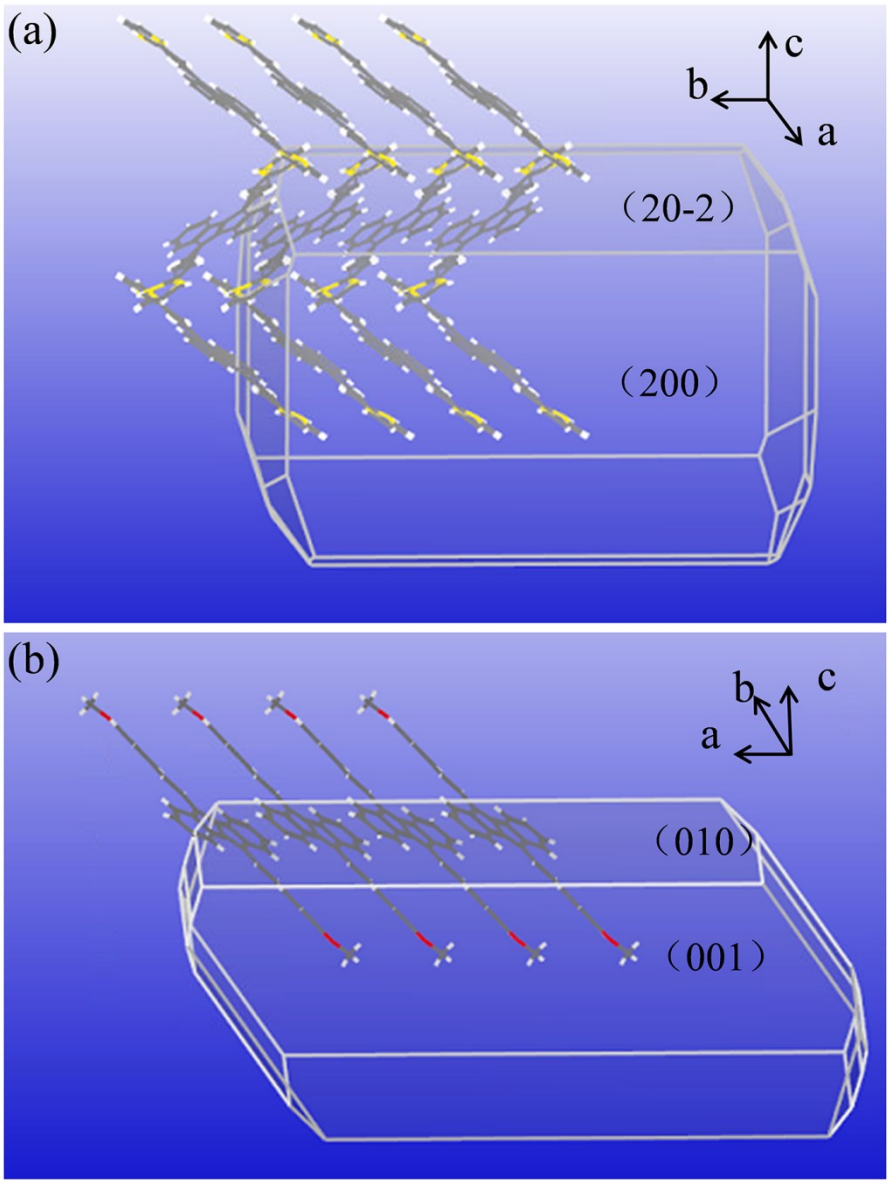

Figure S5 The simulated growth morphologies of TEP crystal (a) and OSDP one (b) using Materials Studio package. TEP molecules are more inclined to adopt a herringbone packing arrangement while OSDP molecules like to adopt a typical 2D-lamellar stacking arrangement in MRs.

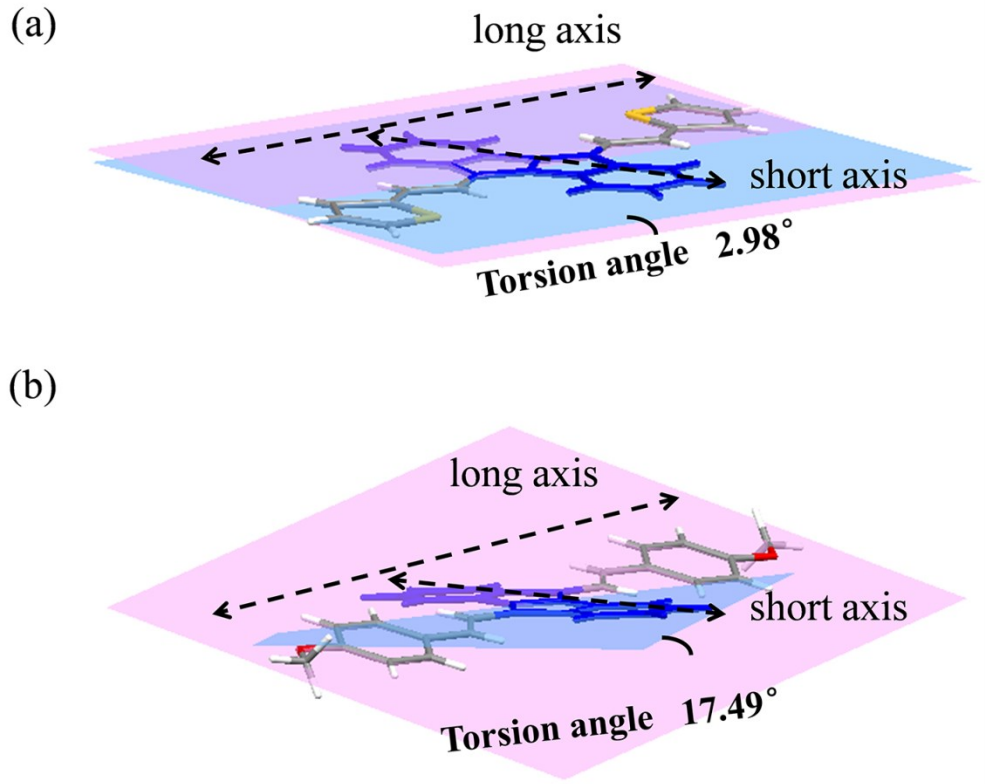

Figure S6 (a) Molecular length of TEP with small torsion angle of 2.98°. (b) Molecular length of OSDP with larger torsion angle of 17.49°. We define DBP skeleton direction as short axis and another as long axis.

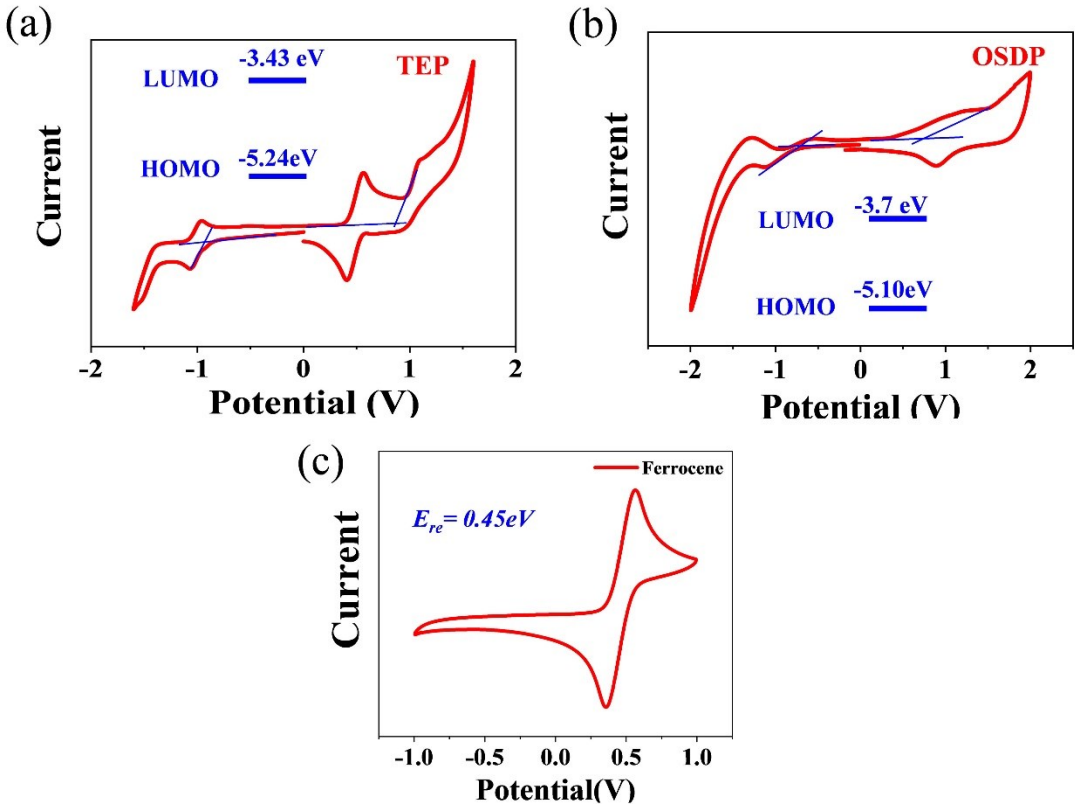

Figure S7 Cyclic voltammetry measurement of TEP (a) and OSDP compounds (b) in the acetonitrile solution. (c) Cyclic voltammetry measurement of ferrocene as reference.

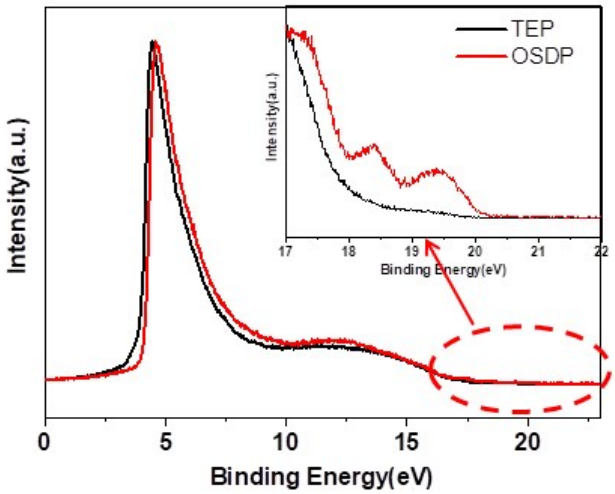

Figure S8 UPS Energy distribution curve of TEP and OSDP thin films. HOMO = hv + E_{cutoff} – E_F; hv = 21.12 eV. TEP: 21.12 - (19.9 - 3.98) = 5.20eV. OSDP: 21.12 - (20.1 - 4.16) = 5.18eV

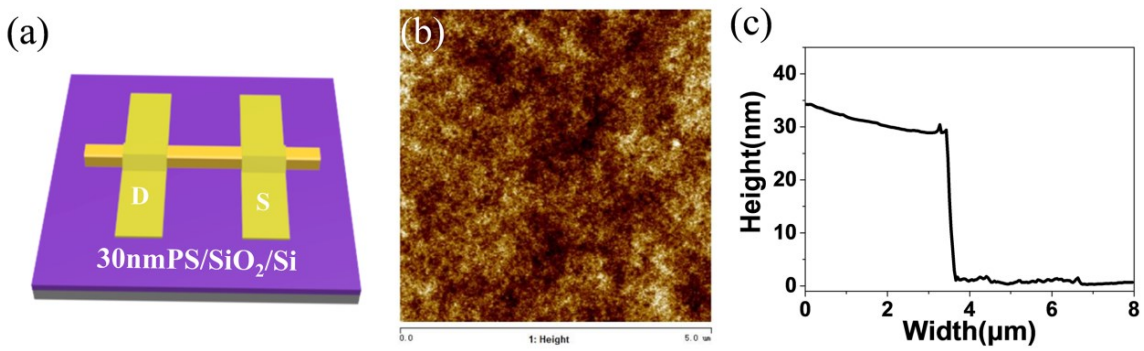

Figure S9 (a) Schematic of two single-crystalline OFETs of TEP and OSDP MRs with bottom-gate top-contact configuration. (b) AFM image of spincoating 30-nm PS-film. (c) The corresponding height sketch of PS film.

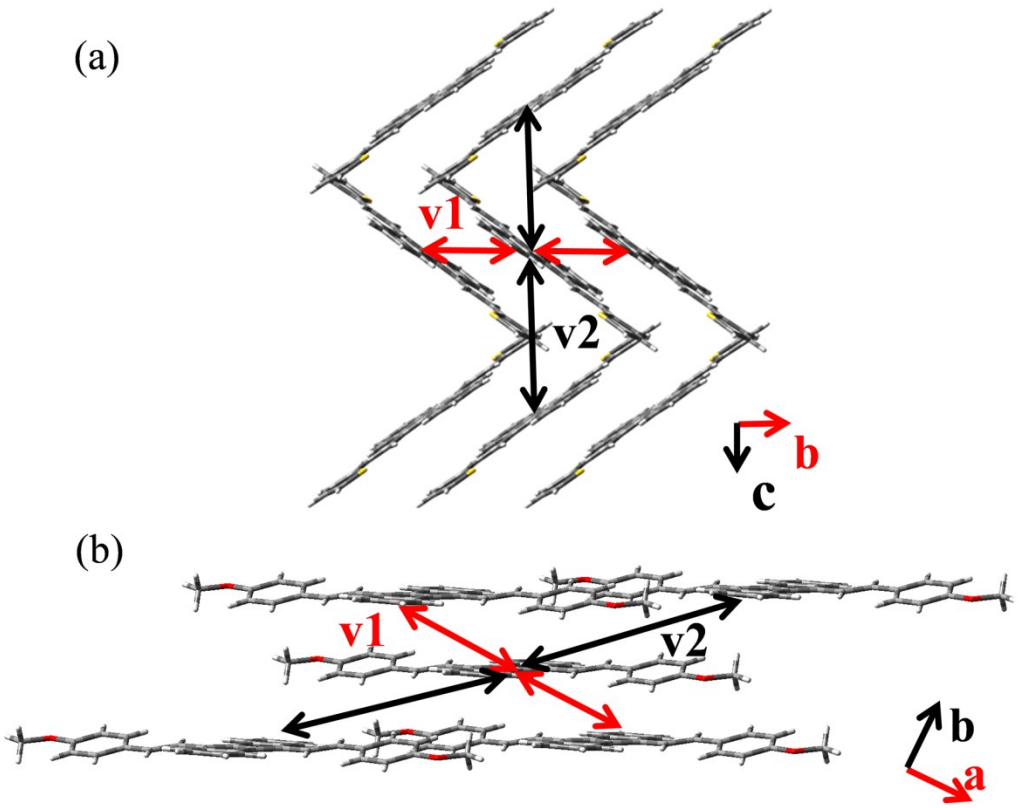

Figure S10 Illustrations of transfer integrals for the nearest neighboring molecular pairs considered in the calculations for TEP (a) and OSDP crystals (b) based on the direct integration with site-energy correction.

Table S2 Theoretic calculation of hole reorganization energy (meV), intermolecular distance and transfer integral (meV) for TEP and OSDP.

Semiconductor	Pathway	d_{c-c} (Å)	Hole transfer integral (mev)	Hole reorganization (mev)
TEP	V1	5.688	43.473	261.52
	V2	8.256	0.218	
OSDP	V1	5.220	42.470	364.96
	V2	12.509	6.536	

The reorganization energies of TEP and OSDP are calculated and shown in Table S2. It is clear that the reorganization energy of TEP (261.52 meV) presents lower than that of OSDP (364.96 meV). This might be ascribed to the smaller π-π distance caused by the coplanar conjugated structure, almost perfect rigid structure and large electronic coupling in TEP. The d_{c-c} is central distance.

The calculated transfer integral of 43.473 meV (V1) in TEP MRs is very close to the value of 42.470 meV in OSDP MRs. However, the transfer integrals of the other pathway are extremely low for both TEP and OSDP.

Computational Details: The transfer integrals for the nearest neighbor dimers along the transport pathways are calculated using the site energy correction method at PW91PW91/6-31G* level. Charge reorganization energies are evaluated by the adiabatic potential energy surfaces (AP) method at B3LYP/6-31G(d) level. All calculations are based on Density Functional Theory (DFT) with Gaussian09 package.

Table S3 Comparison the linear mobility with the saturated mobility.

	The linear mobility $cm^2 V^{-1} s^{-1}$	The saturated mobility $cm^2 V^{-1} s^{-1}$
TEP	0.43	1.02 (figure 4a)
	0.25	0.40
	0.31	0.67
OSDP	0.009	0.11(figure 4b)
	0.0087	0.05
	0.0052	0.07

The mobility in the saturation region was calculated by using the following equation:

$$\mu_{sat} = 2L\left(\partial\sqrt{I_{DS}}/\partial V_{GS}\right)^2/WC_i$$ (applicable at $|V_G - V_T| < |V_{DS}|$).

The mobility in the linear region was calculated by using of the following equation:

$$\mu_{lin} = L(\partial I_{DS}/\partial V_G)/WC_iV_{DS}$$ (applicable at $|V_G - V_T| \gg |V_{DS}|$)

Therefore, we obtain the linear mobility values of different devices and list the typical data in the table aimed to comparing the saturated and linear mobility values.